

Advanced ACTPol Cryogenic Detector Arrays and Readout

S. W. Henderson¹ · R. Allison² · J. Austermann³ · T. Baildon⁴ · N. Battaglia⁵ · J. A. Beall³ · D. Becker³ · F. De Bernardis¹ · J. R. Bond⁶ · E. Calabrese⁵ · S. K. Choi⁷ · K. P. Coughlin⁴ · K. T. Crowley⁷ · R. Datta⁴ · M. J. Devlin⁸ · S. M. Duff³ · J. Dunkley² · R. Dünner⁹ · A. van Engelen⁶ · P. A. Gallardo¹ · E. Grace⁷ · M. Hasselfield⁵ · F. Hills⁴ · G. C. Hilton³ · A. D. Hincks¹⁰ · R. Hložek⁵ · S. P. Ho⁷ · J. Hubmayr³ · K. Huffenberger¹¹ · J. P. Hughes¹² · K. D. Irwin¹³ · B. J. Koopman¹ · A. B. Kosowsky¹⁴ · D. Li^{3,15} · J. McMahon⁴ · C. Munson⁴ · F. Nati⁸ · L. Newburgh¹⁶ · M. D. Niemack¹ · P. Niraula⁷ · L. A. Page⁷ · C. G. Pappas⁷ · M. Salatino⁷ · A. Schillaci^{7,22} · B. L. Schmitt⁸ · N. Sehgal¹⁷ · B. D. Sherwin¹⁸ · J. L. Sievers¹⁹ · S. M. Simon⁷ · D. N. Spergel⁵ · S. T. Staggs⁷ · J. R. Stevens¹ · R. Thornton²⁰ · J. Van Lanen³ · E. M. Vavagiakis¹ · J. T. Ward⁸ · E. J. Wollack²¹

Received: 29 September 2015 / Accepted: 2 March 2016 / Published online: 28 March 2016
© Springer Science+Business Media New York 2016

Abstract Advanced ACTPol is a polarization-sensitive upgrade for the 6 m aperture Atacama Cosmology Telescope, adding new frequencies and increasing sensitivity over the previous ACTPol receiver. In 2016, Advanced ACTPol will begin to map approximately half the sky in five frequency bands (28–230 GHz). Its maps of primary and secondary cosmic microwave background anisotropies—imaged in intensity and polarization at few arcminute-scale resolution—will enable precision cosmological constraints and also a wide array of cross-correlation science that probes the expansion history of the universe and the growth of structure via gravitational collapse. To accomplish these scientific goals, the Advanced ACTPol receiver will be a significant upgrade to the ACTPol receiver, including four new multichroic arrays of cryogenic, feedhorn-

✉ S. W. Henderson
swh76@cornell.edu

¹ Department of Physics, Cornell University, Ithaca, NY 14853, USA

² Sub-Department of Astrophysics, University of Oxford, Keble Road, Oxford OX1 3RH, UK

³ NIST Quantum Devices Group, 325 Broadway Mailcode 817.03, Boulder, CO 80305, USA

⁴ Department of Physics, University of Michigan, Ann Arbor 48103, USA

⁵ Department of Astrophysical Sciences, Peyton Hall, Princeton University, Princeton, NJ 08544, USA

coupled AlMn transition edge sensor polarimeters (fabricated on 150 mm diameter wafers); a system of continuously rotating meta-material silicon half-wave plates; and a new multiplexing readout architecture which uses superconducting quantum interference devices and time division to achieve a 64-row multiplexing factor. Here we present the status and scientific goals of the Advanced ACTPol instrument, emphasizing the design and implementation of the Advanced ACTPol cryogenic detector arrays.

Keywords Bolometers · Cosmic microwave background · Millimeter-wave · Polarimetry · Superconducting detectors · Transition edge sensors

1 Introduction

A worldwide experimental effort is underway to map the polarization of the CMB (see, for example [1–9]). These measurements will provide constraints on the parameters of the standard Λ CDM model that are independent of those obtained from the CMB temperature alone. Moreover, the parameters may be more tightly constrained by the former due to the higher contrast of the acoustic features in polarization

-
- ⁶ Canadian Institute for Theoretical Astrophysics, University of Toronto, Toronto, ON M5S 3H8, Canada
 - ⁷ Joseph Henry Laboratories of Physics, Jadwin Hall, Princeton University, Princeton, NJ 08544, USA
 - ⁸ Department of Physics and Astronomy, University of Pennsylvania, 209 South 33rd Street, Philadelphia, PA 19104, USA
 - ⁹ Departamento de Astronomía y Astrofísica, Pontificia Universidad Católica, Casilla 306, Santiago 22, Chile
 - ¹⁰ Department of Physics and Astronomy, University of British Columbia, Vancouver, BC V6T 1Z4, Canada
 - ¹¹ Department of Physics, Florida State University, Tallahassee, FL 32306, USA
 - ¹² Department of Physics and Astronomy, Rutgers, The State University of New Jersey, Piscataway, NJ 08854-8019, USA
 - ¹³ Department of Physics, Stanford University, Stanford, CA 94305-4085, USA
 - ¹⁴ Department of Physics and Astronomy, University of Pittsburgh, Pittsburgh, PA 15260, USA
 - ¹⁵ SLAC National Accelerator Laboratory, 2575 Sandy Hill Road, Menlo Park, CA 94025, USA
 - ¹⁶ Dunlap Institute, University of Toronto, 50 St. George St., Toronto, ON M5S 3H4, Canada
 - ¹⁷ Physics and Astronomy Department, Stony Brook University, Stony Brook, NY 11794, USA
 - ¹⁸ Berkeley Center for Cosmological Physics, University of California, Berkeley, CA 94720, USA
 - ¹⁹ Astrophysics and Cosmology Research Unit, School of Mathematics, Statistics and Computer Science, University of KwaZulu-Natal, Durban 4041, South Africa
 - ²⁰ Department of Physics, West Chester University of Pennsylvania, West Chester, PA 19383, USA
 - ²¹ NASA Goddard Space Flight Center, Greenbelt, MD 20771, USA
 - ²² Sociedad Radiosky Asesorías de Ingeniería Limitada Lincoyán 54, Depto 805, Concepción, Chile

compared to astrophysical foregrounds [10,11]. CMB polarization also probes multiple types of physics beyond the standard model, including measuring the sum of the neutrino masses ($\sum m_\nu$) and constraining the tensor-to-scalar ratio of primordial fluctuations (r). The polarization anisotropies in the CMB are more than an order of magnitude fainter than the temperature anisotropies, requiring large arrays of detectors integrating over long periods of time to detect them. Optimized low-temperature detectors are photon-background limited over the CMB frequency bands accessible from the ground, making them well-suited to these observations. Substantial progress has been made in this field in the last two years, with ground-based experiments reporting the first high-significance detections of numerous new signals including so-called “B-mode” polarization at both small (sub-degree) [12] and large (degree) [13] angular scales. Current ground-based efforts include instruments such as the Atacama Cosmology Telescope Polarization-sensitive receiver (ACTPol) [1], Polarbear [4], SPTPol [5], BICEP2 [2], Keck-array [3], and CLASS [9]. This paper describes Advanced ACTPol (AdvACT), an upgrade to the ACTPol receiver. ACTPol has demonstrated near-photon-background limited operation in its published scientific results from its first season [14–18], and has presented preliminary results from its second and third seasons [19,20].

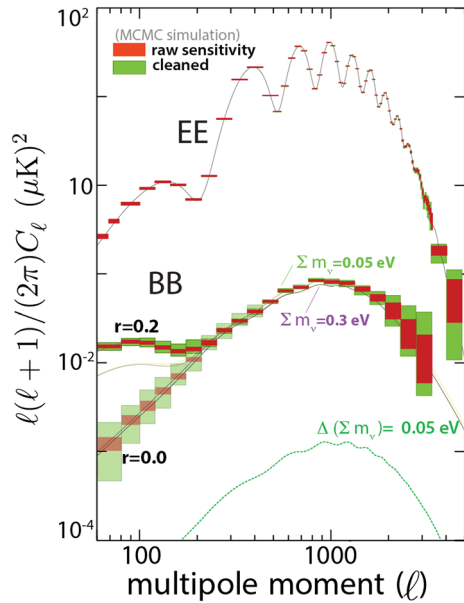
In Sect. 2 we present the scientific objectives of the AdvACT upgrade and in Sect. 3 we describe the instrumental upgrades designed to achieve these objectives, and we conclude in Sect. 4 with a discussion of the status and future of the experiment.

2 Scientific Objectives and Motivation

With AdvACT we plan to map approximately half of the microwave sky in five frequency bands spanning from 28 to 230 GHz with four new arrays of detectors. In addition to extended spectral coverage, AdvACT will have excellent angular resolution (expected: $1.4'$ at 150 GHz, $7.1'$ at 28 GHz), and increased polarization and temperature sensitivity as a result of roughly doubling the number of detectors per array in the mid- and high-frequency optical bands relative to ACTPol. Polarization systematics and low-frequency receiver noise will be controlled with the use of ambient temperature continuously rotating metamaterial silicon half-wave plates (HWPs), which will modulate the incoming polarized signals at ~ 8 Hz, improving access to the large angular scale signals expected from inflation.

With these advances in sensitivity and systematics, we anticipate that measurements with AdvACT will substantially improve our understanding of cosmology, nearly halving the uncertainty on many basic cosmological parameters including the baryon and matter densities, $\Omega_b h^2$ and $\Omega_c h^2$, as well as the spectral index n_s . The wide spectral coverage from the AdvACT arrays, combined with existing *Planck* 353 GHz maps, has been chosen for efficiently detecting and removing synchrotron and dust foregrounds, targeting a cosmic variance-limited measurement of the primordial CMB polarization out to $\ell = 2000$. The large AdvACT survey region has been selected to increase the sensitivity for inflationary gravity wave searches and permit measurements of the isotropy, frequency spectrum, and scale dependence of any detected signal. Figure 1 shows the predicted errors on *EE*- and *BB*-mode power spectra expected for the

Fig. 1 Forecast AdvACT errors on E E and B B spectra, compared to Λ CDM predictions, for several values of r and $\sum m_\nu$. The red error bars indicate the raw sensitivity. The green error bars indicate an estimate for the degradation due to cleaning foregrounds that approximate Planck data ($3\times$ dustier than the nominal PSM), based on fitting a simple blackbody CMB plus power-law dust and synchrotron model in each degree-scale patch. This foreground projection is estimated to increase the map noise level to $\approx 10\text{--}12\ \mu\text{K}\text{-arcmin}$, although in practice the noise increase is expected to have scale dependence (Color figure online)



complete AdvACT campaign, as compared with the spectra expected for different values of r and $\sum m_\nu$. The red boxes show projected errors on the power spectra based on the predicted AdvACT raw instrument sensitivity, while the green boxes show projections after using the wide spectral coverage of AdvACT in conjunction with Planck measurements at 353 GHz to remove dust foregrounds three times larger than in the Planck Sky Model (PSM) [21].

The measurements with AdvACT of secondary CMB anisotropies such as the thermal and kinematic Sunyaev–Zel’dovich effects (tSZ and kSZ) [22, 23] and gravitational lensing [24], will map the dark matter distribution, and potentially provide a high signal-to-noise measurement of the sum of the neutrino masses. In addition, AdvACT precision E E data will provide an independent measurement of the primordial T T spectrum, allowing for a detection of the homogenous kSZ effect at $>10\sigma$ in AdvACT T T data [11].

AdvACT benefits from extensive overlap with a large number of other existing and planned surveys, including the Large Synoptic Survey Telescope (LSST) [25], as well as other optical surveys like HSC [26] and DES [27], X-ray surveys like eROSITA [28], and spectroscopic surveys like SDSS-III [29] and DESI [30]. This enables a wide array of cross-correlation science probing different epochs and is projected to result in the detection of $>10,000$ galaxy clusters at 99 % purity via their tSZ signatures and $\sim 10,000$ high redshift, lensed, millimeter sources.

3 Instrument Overview

AdvACT will be an upgrade of ACTPol’s three existing detector arrays and their optics, staged over three years. The AdvACT receivers will be deployed on the existing Ata-

Table 1 Receiver parameters and projected sensitivity

Detector array	Center freq. (GHz)	Width (GHz)	# TES –	Projected map noise ($\mu\text{K-arcmin}$)	Beam size (arcmin)
LF	28	6	88	80	7.1
LF	41	19	88	70	4.8
MF	90	39	1712	8	2.2
MF/HF	150	41	2718	7	1.4
HF	230	100	1006	25	0.9

In total, AdvACT will deploy four new multichroic arrays; a high-frequency (HF) array operating at 150 and 230 GHz, two medium frequency (MF) arrays operating at 90 and 150 GHz, and a low-frequency (LF) array operating at 28 and 41 GHz. Map noise levels are based on three full years of observations, and are given in CMB temperature units (multiply by $\sqrt{2}$ for polarization)

cama Cosmology Telescope [31], located at 5190 m elevation in Parque Astronómico Atacama in northern Chile. AdvACT will reuse ACTPol’s dilution refrigerator cryostat, which enables continuous $\simeq 100$ mK observation. The ACT telescope focuses sub-mm radiation onto each of three optics tubes in the cryostat, each of which contains a chain of filters and cold silicon reimaging optics which focus the radiation onto monolithic silicon feedhorn arrays directly coupled to arrays of transition-edge sensor (TES) bolometers. AdvACT will deploy four new multichroic arrays, as summarized in Table 1. As described in the following sections, the densely packed AdvACT multichroic detector arrays require significant upgrades to the receiver optics, detectors, and readout to obtain the required bandwidth and polarization sensitivity.

3.1 Optics

The AdvACT receiver is located at the Gregorian focus of the ACT telescope. Each multichroic optics tube will have an ambient temperature metamaterial silicon half-wave plate (HWP) located in front of the optics tube window, optimized for its multichroic array bandpass. The HWPs are rotated at ~ 2 Hz on custom air-bearing rotors, modulating the incoming polarization at ~ 8 Hz. Each HWP will be comprised of a stack of silicon wafers with machined grooves which together behave as an achromatic, birefringent material. The Atacama B-Mode Search (ABS) has demonstrated a reduction of low-frequency atmospheric noise amplitude by a factor of greater than 500 using a sapphire HWP, with less than 0.1 % leakage of intensity to polarization [32]. The metamaterial silicon HWPs for AdvACT will be twice as birefringent as sapphire, resulting in substantially less loss. The broad-band configuration will consist of a stack of three rotated HWPs [33] sandwiched between two additional silicon layers with grooved metamaterial AR coatings.

After the HWPs, light is focused by cryogenic silicon lenses onto a gold-plated silicon micro-machined platelet array of feedhorns, also optimized for the bandpass of its multichroic array. The silicon lenses for each array have frequency matched, broad-band AR metamaterial coatings consisting of three layers of grooves, proven to have negligible in-band dielectric loss and reflection and excellent polarization symmetry [35]. The feedhorns are a new broad-band, spline-profiled smooth-wall

TES	150A/B	230A/B
AASP5 R_n (m Ω)	7.0 \pm 0.5	7.4 \pm 0.2
AASP6 R_n (m Ω)	7.6 \pm 0.1	7.5 \pm 0.6
Target R_n (mΩ)	8	
AASP5 T_c (mK)	178 \pm 1	177 \pm 1
AASP6 T_c (mK)	182 \pm 2	182 \pm 2
Target T_c (mK)	160	
AASP5 P_{sat} (pW)	12.7 \pm 0.9	24.3 \pm 0.6
AASP6 P_{sat} (pW)	14.1 \pm 0.8	28 \pm 3
Target P_{sat} (pW)	12.5	25
AASP5 G (pW/K)	247 \pm 16	557 \pm 11
AASP6 G (pW/K)	262 \pm 16	580 \pm 35
Target G (pW/K)	268	536
Leg Width (μ m)	14.5	28.5

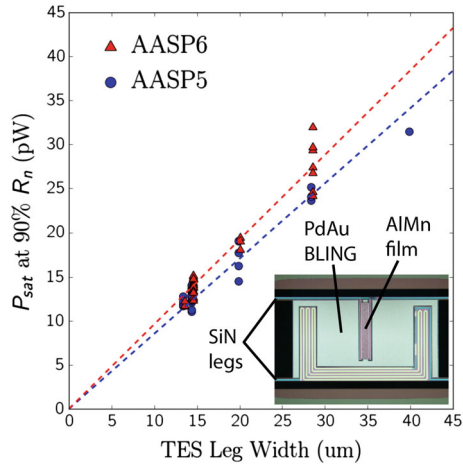


Fig. 2 *Left* Measured average and RMS AdvACT detector parameters for many HF single pixels fabricated on two 75 mm test wafers, AASP5 and AASP6, as compared with targeted values. R_n is the AIMn film normal resistance, T_c the transition temperature, P_{sat} the electrical bias power at 90% R_n , and G the thermal conductance to the bath at T_c . *Right* P_{sat} versus SiN leg width for typical HF 230/150 and MF 90 GHz devices. *Right inset* A microscope image of an AdvACT AIMn TES [34] (Color figure online)

design, optimized to produce symmetric beams with high coupling-efficiency and low cross-polarization over the large bandwidths required by the AdvACT multichroic arrays. Figure 3 shows the first completed AdvACT feedhorn array.

3.2 Detectors

Each feed horn focuses light onto a single pixel, where it is coupled via planar superconducting microwave on-chip circuitry to four TES bolometers: two for each linear polarization state and two for each frequency band [36]. ACTPol has recently successfully deployed the first multichroic array for a CMB experiment, operating at 90 and 150 GHz [19,20]. Instead of tiling 75 mm wafers to form each full array as in ACTPol, each AdvACT array will be fabricated on a single, 150 mm diameter, 500 μ m thick silicon wafer, allowing for more efficient packing of the ACT focal plane and higher pixel densities [37].

The AdvACT TESes are fabricated from single-layer AIMn films instead of bilayer MoCu films as in ACTPol [38]. Several rounds of single-pixel MF and HF prototypes have been successfully fabricated that meet the target specifications for AdvACT [34, 39]. The results of extensive electrical and thermal characterization of HF devices from single pixels fabricated on two 75 mm test wafers are compared to targeted parameters in Fig. 2 and its table.

3.3 Readout

Each TES in the AdvACT arrays will be DC voltage biased, and each array will be read out via a time division multiplexing (TDM) scheme as implemented in the warm

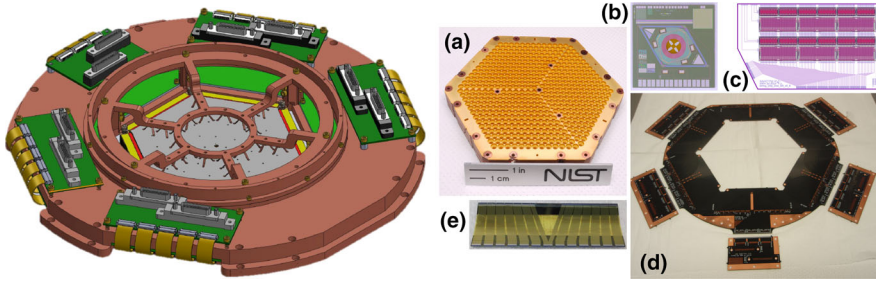


Fig. 3 *Left* 3D model of the AdvACT HF array package. The full array assembly is enclosed within a 100 mK OHFC copper shield. *Right a* HF silicon micro-machined feedhorn array. **b** AdvACT HF test pixel. **c** Layout for one of eight wiring chips that distribute TES signals from the array to the SQUID MUX, with MUX and detector bias chips overlaid. **d** Six-layer PCBs that route signals from MCE to wiring chips. **e** Superconducting flex interface between HF array and main ring-shaped PCB (Color figure online)

Multi-Channel Electronics (MCE) [40]. The high TES density in the MF and HF arrays will require a multiplexing (MUX) factor, or number of detectors per readout channel, of 64:1, substantially larger than the highest MCE MUX factor yet of 41:1 implemented on SCUBA2 [41]. We have already demonstrated all the required electronics capabilities for a 64:1 MUX factor while reading out an 11 column by 44-row array of SQUIDs in the laboratory.

The arrays will be multiplexed through the MCE using a new TDM MUX architecture developed at NIST/Boulder with two SQUID stages and flux activated SQUID switches [42, 43]. The current in each TES in the array is inductively coupled to its own first-stage SQUID (SQ1) and operated in a flux-locked loop that acts on the output of a second stage SQUID series array. New cryogenic interfaces have been developed to connect each TES in the AdvACT arrays at 100 mK into this cold MUX circuit.

At 100 mK, signal pairs from each TES are carried to its own SQ1 via superconducting Nb traces on the wafer Al bonded to flexible ribbon cable containing superconducting Al traces. The voltage biasing is routed such that TESes observing at different optical frequencies are wired to different voltage bias lines and TESes from polarization pairs at one optical frequency for a given pixel are read out through the same 4 K SQUID series array and 300 K warm amplifier. The SQ1s and associated wiring and addressing chips are located on a large printed circuit board (PCB) which surrounds the array. It contains routing and bondpads to the appropriate silicon chips for all necessary control lines: TES biases, SQUID biases and feedbacks, and switching currents. In total, the AdvACT MF and HF arrays will each require in excess of 20,000 aluminum wirebonds, and numerous new tools and procedures have been developed to ensure a robust and high yield integration [44]. The entire AdvACT HF array mechanical and readout 100 mK assembly is shown in Fig. 3.

4 Status

Observations with the first AdvACT array will begin in 2016, replacing one of the ACTPol arrays with the 150/230 GHz AdvACT HF array. The staged deployment of the additional AdvACT arrays is planned for 2017 and 2018.

Acknowledgments This work was supported by the U.S. National Science Foundation through Awards 1312380 and 1440226. The NIST authors would like to acknowledge the support of the NIST Quantum Initiative. The development of multichroic detectors and lenses was supported by NASA Grants NNX13AE56G and NNX14AB58G. The work of KPC, KTC, EG, BJK, CM, BLS, JTW, and SMS was supported by NASA Space Technology Research Fellowship awards.

References

1. M.D. Niemack et al., Proc. SPIE **7741**, 77411S (2010)
2. P.A.R. Ade et al., *Astrophys. J.* **792**, 62 (2014). doi:[10.1088/0004-637X/792/1/62](https://doi.org/10.1088/0004-637X/792/1/62)
3. Z. Staniszewski et al., *J. Low Temp. Phys.* **167**, 827 (2012). doi:[10.1007/s10909-012-0510-1](https://doi.org/10.1007/s10909-012-0510-1)
4. K. Arnold et al., Proc. SPIE **7741**, 77411E (2010)
5. J.E. Austermann et al., Proc. SPIE **8452**, 84521E (2012)
6. W. Grainger et al., Proc. SPIE **7020**, 70202N (2008)
7. A. Fraisse et al., *JCAP* **2013**(04), 047 (2013). doi:[10.1088/1475-7516/2013/04/047](https://doi.org/10.1088/1475-7516/2013/04/047)
8. J.A. Tauber et al., *A&A* **520**, A1 (2010). doi:[10.1051/0004-6361/200912983](https://doi.org/10.1051/0004-6361/200912983)
9. T. Essinger-Hileman et al., Proc. SPIE **9153**, 91531I (2014)
10. S. Galli et al., *Phys. Rev. D* **90**, 063504 (2014). doi:[10.1103/PhysRevD.90.063504](https://doi.org/10.1103/PhysRevD.90.063504)
11. E. Calabrese et al., *JCAP* **2014**(08), 010 (2014). doi:[10.1088/1475-7516/2014/08/010](https://doi.org/10.1088/1475-7516/2014/08/010)
12. D. Hanson et al., *Phys. Rev. Lett.* **111**, 141301 (2013). doi:[10.1103/PhysRevLett.111.141301](https://doi.org/10.1103/PhysRevLett.111.141301)
13. P.A.R. Ade et al., *Phys. Rev. Lett.* **112**, 241101 (2014). doi:[10.1103/PhysRevLett.112.241101](https://doi.org/10.1103/PhysRevLett.112.241101)
14. S. Naess et al., *JCAP* **10**, 007 (2014). doi:[10.1088/1475-7516/2014/10/007](https://doi.org/10.1088/1475-7516/2014/10/007)
15. M. Madhavacheril et al., *Phys. Rev. Lett.* **114**, 151302 (2015). doi:[10.1103/PhysRevLett.114.151302](https://doi.org/10.1103/PhysRevLett.114.151302)
16. R. Allison et al., *MNRAS* **451**, 849 (2015). doi:[10.1093/mnras/stv991](https://doi.org/10.1093/mnras/stv991)
17. A. van Engelen et al., *Astrophys. J.* **808**(1), 7 (2015). doi:[10.1088/0004-637X/808/1/7](https://doi.org/10.1088/0004-637X/808/1/7)
18. E. Grace et al., Proc. SPIE **9153**, 91531O (2014)
19. S.P. Ho, et al., In this Special Issue LTD16 in *J. Low Temp. Phys*
20. R. Datta et al., In this Special Issue LTD16 in *J. Low Temp. Phys*
21. J. Delabrouille et al., *A&A* **553**, A96 (2013). doi:[10.1051/0004-6361/201220019](https://doi.org/10.1051/0004-6361/201220019)
22. J.E. Carlstrom, G.P. Holder, E.D. Reese, *Annu. Rev. Astron. Astrophys.* **40**, 643 (2002). doi:[10.1146/annurev.astro.40.060401.093803](https://doi.org/10.1146/annurev.astro.40.060401.093803)
23. E.-M. Mueller et al., *Phys. Rev. D* **92**, 063501 (2015). doi:[10.1103/PhysRevD.92.063501](https://doi.org/10.1103/PhysRevD.92.063501)
24. K.M. Smith et al., *AIP Conf. Proc.* **1141**(1), 121 (2009)
25. Z. Ivezic et al., [arXiv:0805.2366](https://arxiv.org/abs/0805.2366) (2008)
26. S. Miyazaki et al., Proc. SPIE **6269**, 62690B (2006)
27. B.L. Flaugher et al., Proc. SPIE **8446**, 844611 (2012)
28. A. Merloni et al., [arXiv:1209.3114](https://arxiv.org/abs/1209.3114) (2012)
29. K.S. Dawson et al., *Astron. J.* **145**, 10 (2013). doi:[10.1088/0004-6256/145/1/10](https://doi.org/10.1088/0004-6256/145/1/10)
30. M. Levi et al., [arXiv:1308.0847](https://arxiv.org/abs/1308.0847) (2013)
31. D.S. Swetz et al., *Astrophys. J. Suppl. Ser.* **194**(2), 41 (2011). doi:[10.1088/0067-0049/194/2/41](https://doi.org/10.1088/0067-0049/194/2/41)
32. A. Kusaka et al., *Rev. Sci. Instrum.* **85**(2), 024501 (2014). doi:[10.1063/1.4862058](https://doi.org/10.1063/1.4862058)
33. S. Hanany et al., *Appl. Opt.* **44**(22), 4666 (2005). doi:[10.1364/AO.44.004666](https://doi.org/10.1364/AO.44.004666)
34. D. Li et al., In this Special Issue LTD16 in *J. Low Temp. Phys*
35. R. Datta et al., *Appl. Opt.* **52**(36), 8747 (2013). doi:[10.1364/AO.52.008747](https://doi.org/10.1364/AO.52.008747)
36. R. Datta et al., *J. Low Temp. Phys.* **176**(5–6), 670 (2014). doi:[10.1007/s10909-014-1134-4](https://doi.org/10.1007/s10909-014-1134-4)
37. S. Duff et al., In this Special Issue LTD16 in *J. Low Temp. Phys*
38. S.W. Deiker et al., *Appl. Phys. Lett.* **85**(11), 2137 (2004). doi:[10.1063/1.1789575](https://doi.org/10.1063/1.1789575)
39. J. Austermann et al., In this Special Issue LTD16 in *J. Low Temp. Phys*
40. E. Battistelli et al., *J. Low Temp. Phys.* **151**(3–4), 908 (2008). doi:[10.1007/s10909-008-9772-z](https://doi.org/10.1007/s10909-008-9772-z)
41. W.S. Holland et al., *MNRAS* **430**, 2513 (2013). doi:[10.1093/mnras/sts612](https://doi.org/10.1093/mnras/sts612)
42. J. Beyer, D. Drung, *Supercond. Sci. Technol.* **21**(10), 105022 (2008)
43. R. Doriese et al., In this Special Issue LTD16 in *J. Low Temp. Phys*
44. C. Pappas et al., In this Special Issue LTD16 in *J. Low Temp. Phys*